Li, Y P, T Zielinska, M H Jr Ang and W Lin, "Vehicle dynamics of redundant mobile robots with powered caster wheels". *Proceedings of the Sixteenth CISM_IFToMM Symposium, Romansy 16, Robot Design, Dynamics and Control*, ed. Teresa Zielinska and Cezary Zielinski (2006): 221-228.Warsaw: Springer. (Romansy 16 Robot Design, Dynamics and Control, 21 _ 24 Jun 2006,WarsawUniversityofTechnology,Warsaw,Poland)

Vehicle Dynamics of Redundant Mobile Robots with Powered Caster Wheels

Yuan Ping Li* and Teresa Zielinska† and Marcelo H. Ang Jr.* and Wei Lin‡

* National University of Singapore, Faculty of Engineering, Singapore,
e-mail: {liyuanping,mpeangh}@nus.edu.sg

† Warsaw University of Technology, Faculty of Power and Aeronautical Engineering, Poland,
e-mail: teresaz@meil.pw.edu.pl

‡ Singapore Institute of Manufacturing Technology, Singapore,
e-mail: wlin@SIMTech.a-star.edu.sg

Abstract. The dynamic model of redundantly actuated mobile robots with powered caster wheels is derived based on vehicle dynamics. The contact stability problem of wheeled mobile robots is introduced and stable contact condition that characterizes the bounds of contact stability is derived. Sliding mode observer is proposed to estimate the robot velocity using wheel angular velocity and joint torque information. Actuation redundancy of the robot is utilized to satisfy the stable contact condition in trajectory tracking applications.

1 Introduction

More and more important applications of wheeled mobile robots (WMRs) e.g. planetary exploration and mobile manipulation, require accurate dynamic models of WMRs in order to achieve high control performance. Most of the previous literature only consider the linkage dynamics of the rigid bodies on the robot and ignore the dynamic effects of wheel-ground interaction by assuming that the wheels are under pure rolling without slipping motion. However, theory of vehicle dynamics (Bekker, 1956; Wong, 2001), a well established discipline in automobiles dealing with dynamic properties of rolling motion, has revealed that different nonlinear dynamic effects and disturbances will be generated in different wheel-ground interaction conditions. Therefore, this paper discusses the dynamic modelling of WMRs taking into account the wheel-ground interaction. Specifically, dynamic effects caused by the phenomenon of slip is mainly analyzed.

Many WMRs with Powered Caster Wheels (PCWs, also known as offset steerable wheels) have been developed (Wada and Mori, 1996; Yi and Kim, 2002; Li et al., 2005) and even commercialized e.g. the Nomadic XR4000 robot (Holmberg and Khatib, 2000). One important benefit of using PCW is that WMRs with PCWs can generate omnidirectional mobility. However, due to the coupling effects between the rolling and offset steering of the wheel, slip phenomenon is more significant in both longitudinal and lateral directions than other type of wheels. Moreover, most of the WMRs with PCWs use redundant actuators to achieve high payload but cause internal forces between wheels

due to the over-constraints in their kinematics. This further magnifies the occurrence of slip phenomenon. These problems are also encountered by us in controlling our omni-directional mobile robot with 4 PCWs as shown in Figure 1. The robot is redundantly actuated as totally 8 actuators on 4 wheels are used to control the robot.

This paper is an extension of the work (Li et al., 2006). In (Li et al., 2006), dynamic modelling of WMRs with PCWs is improved by considering the effect of wheel-ground interaction. In this paper, we further explore the effects of slip ratio, which is one of the main factors of wheel-ground interaction, on the vehicle dynamics. Moreover, we extend the non-slip conditions derived in (Li et al., 2006) to stable contact condition by considering WMRs locomotion as a multifingered grasping task. Without introducing extra sensors, we apply sliding mode observer to estimate the robot velocity by using the wheel angular velocity and joint torque information. Simulation results are presented to demonstrate the effectiveness of the proposed methods.

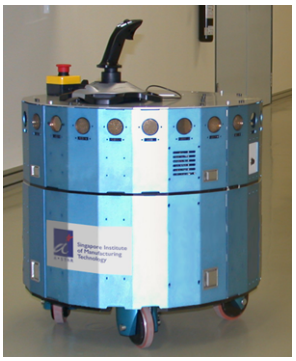

Figure 1. Omnidirectional mobile robot with 4 powered caster wheels.

This paper is organized as follows. Section 2 derives the dynamic model of mobile robots with powered caster wheels using vehicle dynamics. Section 3 introduces the contact stability problem for wheeled mobile robots and derives the stable contact condition to characterize the bounds of contact stability. Simulation results of controlling the robot using the vehicle dynamics model and sliding mode observer are demonstrated in Section 4 followed by the conclusion in Section 5.

2 Dynamics Analysis of WMRs with Powered Caster Wheels

2.1 Vehicle Dynamics

Frame assignments and variable definitions of a WMR with n PCWs is shown in Figure 2. The equations of motion of the overall system can be derived using Operational Space Framework (Khatib, 1987) as

$$\Lambda \ddot{P} + \Phi = GF_c \tag{2.1}$$

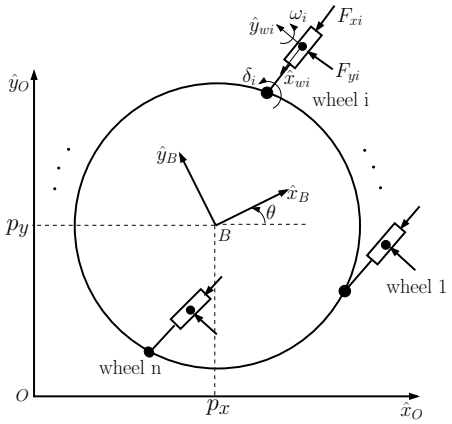

Figure 2. Diagram of a mobile robot with n powered caster wheels.

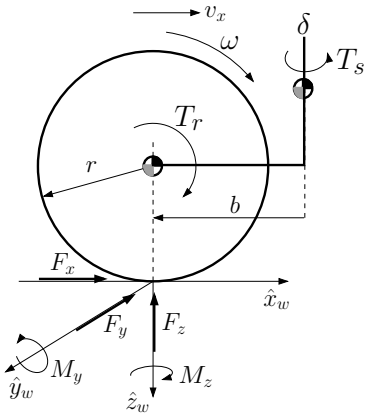

Figure 3. Force equilibrium of a powered caster wheel.

where Λ is the inertial matrix, $P = [p_x, p_y, \theta]^T$ is the operational position and orientation vector of the robot and $\ddot{P}$ is the second derivative of P, Φ is the Coriolis and centrifugal force vector and $F_c = [F_{x1}, F_{y1}, \cdots, F_{xn}, F_{yn}]^T$ is the vector of contact forces. G is the transformation matrix that maps the sum of contact forces into generalized operational forces/torques. Gravitational force is not considered as we assume the robot operates on level ground.

2.2 Wheel Dynamics

Applying the theory of vehicle dynamics (Wong, 2001), the motion and force system of a PCW can be demonstrated with Figure 3. Besides the "normal force" F_z that the ground acts on the robot, the wheel is subjected to longitudinal "tractive force" F_x and "rolling resistance moment" M_y due to the rolling motion. The wheel is also subjected to "lateral force" F_y and "aligning torque" M_z due to the steering motion. The equations of motion of a PCW are given as

$$I_r\dot{\omega} = T_r - M_y - F_x r \tag{2.2}$$

$$I_s\dot{\delta} = T_s - M_z - F_y b \tag{2.3}$$

where I_r and I_s are the inertia tensors of the wheel w.r.t. its rolling and steering axis respectively; ω and δ are the rolling and steering speeds of the wheel respectively; T_r and T_s are the torques of the rolling and steering actuators respectively; r is the radius of the wheel and b is the offset length of the wheel.

Note that the effects of M_y and M_z on the wheel dynamics are usually much smaller than that of the contact forces F_x and F_y, so we will limit our discussion on the contact forces in this paper. Also note that when contact forces F_c are used to relate the vehicle dynamics model (2.1) to the wheel dynamics model (2.2 and 2.3), inertia tensors I_r and I_s should include not only the wheel inertia but also the inertia of the vehicle chassis.

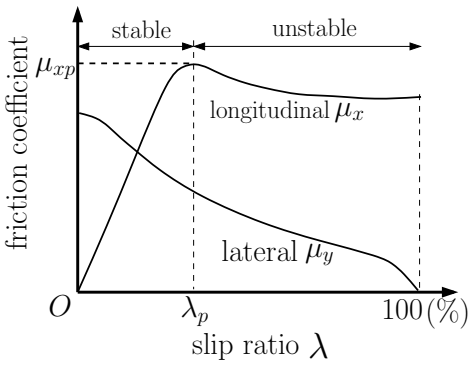

Figure 4. Longitudinal and lateral friction coefficients vary with slip ratio.

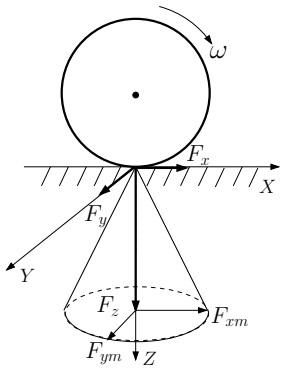

Figure 5. Contact ellipsoid cone of a rolling wheel.

2.3 Relation of Slip Ratio and Contact Force

Contact forces F_x and F_y are usually described in the form of frictional force i.e.

$$F_x = sgn(\omega)\mu_x F_z \hat{x}_w \tag{2.4}$$

$$F_y = -sgn(\delta)\mu_y F_z \hat{y}_w \tag{2.5}$$

where $\hat{x}_w$ and $\hat{y}_w$ are the unit vectors of the wheel frame basis; μ_x and μ_y are defined as longitudinal and lateral friction coefficients which depend mainly on ground conditions and wheel-ground relative motion. The quantity "slip ratio", which characterizes the wheel-ground relative motion, is defined as

$$\lambda = \frac{\omega r - v_x}{max\{\omega r, v_x\}} \times 100\% \tag{2.6}$$

where v_x is the actual longitudinal velocity of the wheel w.r.t. the ground.

Variations of μ_x and μ_y with λ as shown in Figure 4 are important characteristic curves (Wong, 2001) in vehicle dynamics. In the $\mu_x(\lambda)$ curve, μ_x increases with λ until it reaches its peak value μ_{xp} which corresponds to slip ratio λ_p. Further increase of slip ratio beyond λ_p results in rapid decrease of μ_x and the wheel slides or spins on the ground unstably. In the $\mu_y(\lambda)$ curve, μ_y decreases rapidly with increase of λ.

3 Contact Stability of WMRs

WMRs locomotion can be considered as a task where multiple interconnected wheels grasp the ground. This is similar to multifingered grasping tasks where an object is grasped by a multifingered robotic hand. By such an observation, we can consider the "contact stability" problem (Nakamura, 1991) for WMRs as in multifingered grasping tasks. We define contact stability of WMRs locomotion as the ability of the mobile robot to maintain stable rolling contact with the ground when the robot is subjected to

disturbing forces. The problem of "contact stability" is especially important for WMRs because the rolling contact between the wheels and the ground is more sensitive to disturbing forces than static contact which is usually the case for multifingered grasping tasks.

3.1 Stable Contact Condition

It is intuitive to specify conditions that characterize the contact stability of WMRs in terms of contact forces. As shown in Figure 4, maximum longitudinal force F_{xm} is reached when slip ratio is λ_p, and maximum lateral force F_{ym} is reached when slip ratio is zero. Evaluating all possible values of slip ratio, an ellipse with F_{xm} and F_{ym} as the major and minor axes can be obtained. Moreover, evaluating the variation of these ellipses with the normal force F_z, an ellipsoid cone, where a point within the cone corresponds to a stable contact state, can be obtained. We call this "contact ellipsoid cone" as shown in Figure 5. Therefore, a condition characterizing the contact stability is that all contact forces need to be within their contact ellipsoid cones.

Let $f_d = [f_{dx}, f_{dy}]^T$ be the unexpected external disturbing force which is bounded by f_d^*, i.e. $\parallel f_d \parallel \leq f_d^*$. Thus, a stable contact condition can be derived from the concept of contact ellipsoid cone as

$$\frac{(F_{xi} + f_{dx}^*)^2}{F_{xm}^2(F_{zi})} + \frac{(F_{yi} + f_{dy}^*)^2}{F_{ym}^2(F_{zi})} \leq 1 \tag{3.1}$$

Stable contact condition described by Equation 3.1 is a extension of the non-slip conditions derived in the work (Li et al., 2006).

3.2 Contact Force Distribution

In order to satisfy the stable contact condition 3.1, contact force distribution scheme based on the actuation redundancy of the robot can be utilized. A general solution of the vector of contact forces F_c can be derived from Equation 2.1 as

$$F_c = G^{\dagger}(\Lambda \ddot{P} + \Phi) + (I_{2n\times 2n} - G^{\dagger}G) f_o \tag{3.2}$$

where $I_{2n\times 2n}$ is the identity matrix of order $2n$, $G^{\dagger} = G^T(GG^T)^{-1}$ is the pseudo-inverse of matrix G and $f_o \in R^{2n}$ is an arbitrary vector.

In Equation 3.2, the first term in the right hand side corresponds to the contact force components that generate the resultant operational motion of the robot while the second term corresponds to the nullspace of matrix G that generates no effect on the resultant operational motion of the robot. Vector f_o, which is projected onto the nullspace of matrix G, is determined in a way that the final contact forces F_c computed from Equation 3.2 satisfy the stable contact condition 3.1.

4 Sliding Mode Observer

4.1 Observer Design

The evaluation of slip ratio requires information of wheel angular velocity and vehicle actual velocity. In usual cases, sensors are only available to measure wheel angular

velocities and actuator torques. So the vehicle actual velocity needs to be estimated with observers. In a similar application, Unsal and Kachroo (1999) have compared the performances of different nonlinear observers and Sliding Mode Observers was found to provide more satisfactory performance than that of Extended Kalman Filter. The main benefits of sliding mode observers are also well known for their robustness to parametric uncertainty and external disturbances (Slotine and Li, 1991). Therefore, we will adopt sliding mode observer in this paper to estimate the actual velocity of the vehicle.

We first reformulate the system in state space form. We choose state variables as the wheel angular velocity ω and actual velocity of the wheel v_x

$$x = \begin{bmatrix} x_1 \\ x_2 \end{bmatrix} = \begin{bmatrix} \omega \\ v_x \end{bmatrix} \tag{4.1}$$

We can rewrite Equation 2.1,2.2, 2.4 and 2.6 as

$$\begin{array}{rcl} \dot{x}_1 &=& f_1 + gu \\ \dot{x}_2 &=& f_2 \\ y &=& Cx \end{array} \tag{4.2}$$

where

$$\begin{array}{rcl} f_1 &=& -M_y/I_r - \mu_x(x_1, x_2)F_z r/I_r \\ f_2 &=& -\Phi/\Lambda + G\mu_x(x_1, x_2)F_z/\Lambda \\ g &=& 1/I_r \\ u &=& T_s \\ C &=& [1, 0] \end{array} \tag{4.3}$$

Now we can define sliding mode observer as follows

$$\begin{array}{rcl} \dot{\hat{x}}_1 &=& \hat{f}_1 + \hat{g}u - h_1\tilde{y} - k_1 sgn(\tilde{y}) \\ \dot{\hat{x}}_2 &=& \hat{f}_2 - h_2\tilde{y} - k_2 sgn(\tilde{y}) \end{array} \tag{4.4}$$

where $\hat{x}$, $\hat{f}$ and $\hat{g}$ are estimations of x, f and g respectively. Measurement error $\tilde{y} \equiv C(\hat{x} - x)$, observed from the structure of the observer, is chosen as the sliding variable.

Readers are referred to (Slotine et al., 1989) for the details of the observer derivation and its analysis as well as techniques to choose the gains h_1, h_2, k_1 and k_2 so that the estimated states finally match their actual values.

4.2 Application: Simulation Results

We simulated the control diagram of Figure 6 in Matlab. This diagram demonstrate a new control scheme that incorporates the vehicle dynamics model, stable contact condition and sliding mode observer as discussed in this paper.

In the simulation, we commanded the system to track a simple straight line trajectory so that the coupling effects between the longitudinal and lateral dynamics (which are not discussed in this paper) are not generated. In order to generate slip phenomenon and other real effects in the simulation, we introduce random disturbing force with range of $(-0.5F_c, 0.5F_c)$ to the system.

The straight line desired trajectory for the simulation implies that no steering action is involved and only the $\mu_x(\lambda)$ relation is required for the computation of slip ratio in the simulation. For convenience, we adopted following simple model which is proposed in (Peng and Tomizuka, 1990)

$$\mu_x = \frac{2\mu_{xp}\lambda_p\lambda}{\lambda_p^2 + \lambda^2} \tag{4.5}$$

Table 1 shows the parameters and gains of the observer used in the simulation. m_r, m_s and m_c are the mass of the wheel disc, steering link and vehicle chassis respectively.

Table 1. simulation parameters

r	$0.055\ (m)$	b	$0.020(m)$	λ_p	$16(\%)$	μ_{xp}	0.98
m_r	$0.65(kg)$	m_s	$2(kg)$	m_c	$116(kg)$	F_z	$310.5(N)$
h_1	2	h_2	10	k_1	2	k_2	10

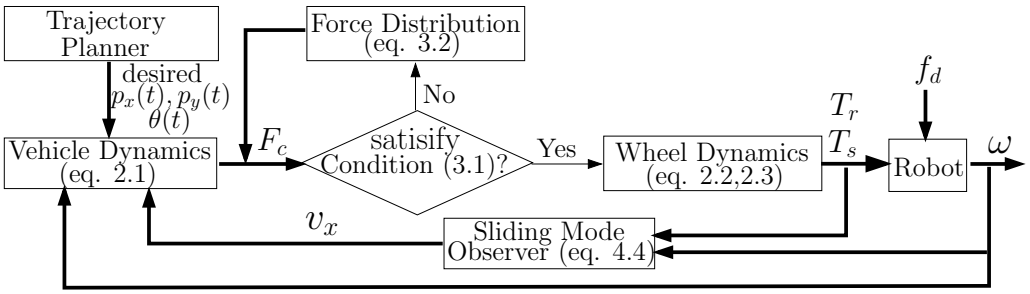

Figure 6. Simulation diagram with sliding mode observer.

Velocity tracking error and estimation error of robot velocity is shown in Figure 7. The tracking error is mainly caused by modelling error and disturbances. Estimation error is relatively small but suffers from chattering. The discussion of chattering elimination is out of the scope of this paper.

Figure 8 shows the actual slip ratio and the estimated slip ratio. It can be noticed that although the slip estimation is effective, the slip ratio is always underestimated by the proposed sliding mode observer.

5 Conclusion

This paper analyzes the vehicle dynamics of wheeled mobile robots with powered caster wheels. Condition that describes the limits of contact stability in terms of contact forces, is derived. Force distribution scheme is proposed to satisfy the stable contact condition. Sliding mode observer is proposed to estimate the system states and its effectiveness is demonstrated by simulation. Future work is to work on the problem of slip based traction control. We also plan to implement the proposed methods on the real robot.

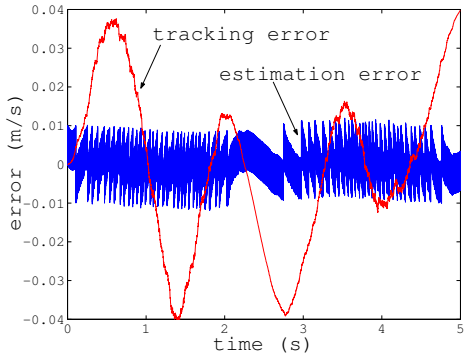

Figure 7. Velocity tracking error and estimation error of robot velocity.

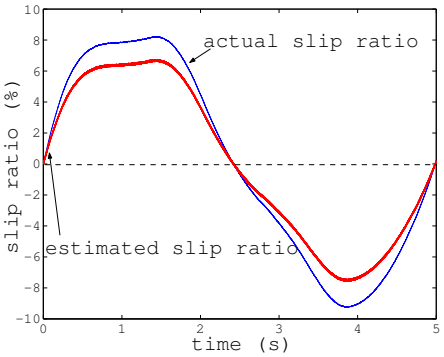

Figure 8. Actual slip ratio and estimated slip ratio.

Bibliography

M.G. Bekker. *Theory of Land Locomotion*. University of Michigan Press, 1956.

R. Holmberg and O. Khatib. Development and control of a holonomic mobile robot for mobile manipulation tasks. *Intl. J. Robotics Research*, 19(11):1066–1074, 2000.

O. Khatib. A unified approach for motion and force control of robot manipulators: The operational space formulation. RA-3(1):43–53, 1987.

Y.P. Li, D.N. Oetomo, Marcelo H. Ang Jr., and C.W. Lim. Torque distribution and slip minimization in an omnidirectional mobile base. *Intl. Conf. Advanced Robotics*, pages 567–572, 2005.

Y.P. Li, T. Zielinska, Marcelo H. Ang Jr., and W. Lin. Wheel-ground interaction modelling and torque distribution for a redundant mobile robot. *IEEE Intl. Conf. Robotics and Automation*, 2006.

Y. Nakamura. *Advanced Robotics: Redundancy and Optimization*. Addison-Wesley Publishing Company, 1991.

H. Peng and M. Tomizuka. Vehicle lateral control for highway automation. *Proc. Amer. Contr. Conf.*, pages 788–794, 1990.

J.-J.E. Slotine, J.K. Hedrick, and E.A. Misawa. On sliding observers for nonlinear systems. *ASME J. Dynamic Syst. Meas. Contr.*, 109:245–252, 1989.

J.-J.E. Slotine and W. Li. *Applied Nonlinear Control*. Prentice Hall, 1991.

Cem Unsal and Pushkin Kachroo. Sliding mode measurement feedback control for antilock braking systems. *IEEE Trans. on Control Systems Technology*, 7(2):271–281, 1999.

M. Wada and S. Mori. Holonomic and omnidirectional vehicle with conventional tires. *Proc. IEEE Intl. Conf. Robotics and Automation*, 4:3671–3676, 1996.

J.Y. Wong. *Theory of Ground Vehicles*. John Wiley and Sons, Inc., 3rd edition, 2001.

B.J. Yi and W.K. Kim. The kinematics for redundantly actuated omni-directional mobile robots. *J. Robotic Systems*, 12(6):255–267, 2002.